NiTi and NiTi-TiC Composites: Part II. Compressive Mechanical Properties

K.L. FUKAMI-USHIRO, D. MARI, and D.C. DUNAND

The deformation behavior under uniaxial compression of NiTi containing 0, 10, and 20 vol pct TiC particulates is investigated both below and above the matrix martensitic transformation temperature: (1) at room temperature, where the martensitic matrix deforms plastically by slip and/or twinning; and (2) at elevated temperature, where plastic deformation of the austenitic matrix takes place by slip and/or formation of stress-induced martensite. The effect of TiC particles on the stress-strain curves of the composites depends upon which of these deformation mechanisms is dominant. First, in the low-strain elastic region, the mismatch between the stiff, elastic particles and the elastic-plastic matrix is relaxed in the composites: (1) by twinning of the martensitic matrix, resulting in a macroscopic twinning yield stress and apparent elastic modulus lower than those predicted by the Eshelby elastic load-transfer theory; and (2) by dislocation slip of the austenitic matrix, thus increasing the transformation yield stress, as compared to a simple load-transfer prediction, because the austenite phase is stabilized by dislocations. Second, in the moderate-strain plastic region where nonslip deformation mechanisms are dominant, mismatch dislocations stabilize the matrix for all samples, thus (1) reducing the extent of twinning in the martensitic samples or (2) reducing the formation of stress-induced martensite in the austenitic samples. This leads to a strengthening of the composites, similar to the strain-hardening effect observed in metal matrix composites deforming solely by slip. Third, in the high-strain region controlled by dislocation slip, weakening of the NiTi composites results, because the matrix contains (1) untwinned martensite or (2) retained austenite, which exhibit lower slip yield stress than twinned or stress-induced martensite, respectively.

I. INTRODUCTION

NEAR-equiatomic NiTi alloys exhibit in the vicinity of room temperature a thermoelastic, allotropic phase transformation between an ordered, high-temperature austenitic phase with B2 cubic structure and an ordered, low-temperature martensitic phase with monoclinic B19' structure. While slip by dislocation motion is activated in these alloys at high applied stresses, other deformation mechanisms can dominate at lower applied stresses: twinning for martensitic NiTi and formation of stress-induced martensite for austenitic NiTi, as reviewed recently in, *e.g.*, References 1 through 8. In both cases, the strain accumulated by these nonslip deformation mechanisms can be fully recovered upon reverse phase transformation to austenite: by temperature-induced transformation upon heating of the twinned martensite (shape-memory recovery) or by stress-induced transformation upon unloading of stress-induced martensite (superelastic recovery). Furthermore, twinned martensite can also exhibit detwinning upon unloading (rubberlike recovery).

As for most other metal matrix composite systems, the presence of a ceramic second phase within the NiTi matrix can result in a composite with decreased density and increased strength, stiffness, hardness, and abrasion resistance.[9] However, unlike composites with matrices deforming solely by slip, the alternative deformation mechanisms described previously (twinning and stress-induced transformation) are expected to be operative in NiTi composites during both the overall deformation of the matrix (driven by the external stress) and its local deformation near the reinforcement (controlled by the mismatch stresses between matrix and reinforcement). An examination of the literature reveals that the influence of internal stresses on the deformation behavior of NiTi-based composites has not been examined by the few investigators who have studied such composites to date. References 10 and 11 characterize the mechanical properties of sintered TiC-NiTi cermets and show that with decreasing TiC content, the hardness and compressive strength decrease, while the ductility and toughness increase. In studying the strengthening and stiffening of aluminum containing continuous and discontinuous NiTi fibers, References 12 and 13 give calculations of the internal stresses resulting from the phase transformation of the fibers. Bidaux *et al.*[14] investigated the temperature dependence of modulus and damping for NiTi wires embedded in an epoxy matrix. Hornbogen and co-workers[15,16] examined the shape-memory effect in silicone-NiTi laminates, for which elastic stresses are stored in the elastomer phase. Finally, Duerig and co-workers[17,18] investigated NiTi-Nb composites formed by eutectic solidification. These composites exhibited an increase in the twinning yield stress of the martensitic matrix, an increase in the transformation hysteresis (further increasing upon deformation), and a decrease in the strain recoverable by shape memory. These observations were explained by the increased friction stress resulting from the plastic deformation of the niobium-rich phase during external loading and shape-memory recovery of the matrix.

K.L. FUKAMI-USHIRO, formerly Graduate Student, Department of Materials Science and Engineering, Massachusetts Institute of Technology, is Development Engineer with Raychem Corp., Menlo Park, CA 94025. D. MARI, formerly Postdoctoral Fellow, Department of Materials Science and Engineering, Massachusetts Institute of Technology, is CEO with Advanced Composite Materials Engineering, 1015 Lausanne, Switzerland. D.C. DUNAND, AMAX Assistant Professor, is with the Department of Materials Science and Engineering, Massachusetts Institute of Technology, Cambridge, MA 02139.

Manuscript submitted March 14, 1995.

The present article is the second in a series investigating the allotropic transformation behavior,[19] the twinning deformation,[20] and the shape-memory recovery[21] of NiTi-based composites containing 10 or 20 vol pct TiC particulates. In the following, we report on the macroscopic deformation behavior of NiTi-TiC composites up to high compressive strains, as functions of TiC content and deformation temperature. The goal is to examine metal matrix composites with deformation mechanisms other than slip (*i.e.*, twinning at room temperature and stress-induced transformation at elevated temperature) with particular emphasis on the effect of mismatch between the stiff, elastic particles and the elastically and plastically deforming matrix. We note that the present study is also relevant to other composites with matrices deforming by nonslip mechanisms: twinning is common in, *e.g.*, tin, zinc, magnesium, brass, and iron,[22] and deformation by stress-induced transformation occurs in, *e.g.*, cobalt and steels, and contributes to toughening of transformation-induced plasticity steels and WC-Co cermets.[23–26]

II. EXPERIMENTAL PROCEDURES

Prealloyed NiTi powders (99.9 pct pure, 70-μm average size, from Special Metals Corp., New Hartford, NY) were mixed with 0, 10, and 20 vol pct TiC particles (99.5 pct pure, between 44 and 100 μm in size, from Cerac, Inc., Milwaukee, WI). The powder mixtures, separated by graphite discs coated with boron nitride, were poured into a graphite die lined with a boron-nitride coated titanium foil and vacuum hot-pressed at 1353 K under pressures of 65 to 75 MPa for 4 to 6 hours. The specimens, respectively labeled in what follows NiTi, NiTi-10TiC, and NiTi-20TiC, were then hot-isostatically pressed with 99.999 pct pure argon at 1433 K under a pressure of 172 MPa for 2 hours without encapsulation.

Calorimetry samples were cut from the consolidated specimens with a low-speed diamond saw. To eliminate residual stresses induced by cutting and to homogenize the microstructure, the samples were annealed in a titanium-gettered, 99.9 pct pure argon atmosphere at 1203 K for 1 hour, furnace-cooled to 673 K at an average rate of 4.5 K·min^{-1}, and air-cooled to room temperature at approximately 20 K·min^{-1}. Transformation temperatures were measured by differential scanning calorimetry with a PERKIN-ELMER*

*PERKIN-ELMER is a trademark of Perkin-Elmer Physical Electronics, Eden Prairie, MN.

DSC-7 calorimeter at a rate of 3 K·min^{-1} under nitrogen cover gas. Metallographic preparation consisted of polishing with 4000 grit SiC paper followed by etching for 15 to 20 seconds in a solution of 1 part HF, 4 parts HNO_3, and 5 parts H_2O.

Two batches of right parallelepiped compression samples were cut from the consolidated specimens by electrodischarge machining and annealed as described previously. Sample dimensions were 5 × 5 × 12.7 mm for batch 1 and 5 × 5 × 10 mm for batch 2, with tolerances within 5 μm of the nominal dimensions and within 0.25 deg of orthogonality. Samples were deformed in compression between steel disks with graphite-lubricated carbide inserts at a crosshead speed of 1 μm·s^{-1}. For room-temperature tests up to strains of 2 pct, strain was measured by two 1.57-mm strain gages mounted on opposite sides of the specimens. For deformation to strains higher than 2 pct and for tests at elevated temperature, a linear variable displacement transducer (LVDT) measured displacement of the inner faces of the steel discs. Strains were calculated after correcting for the elastic deformation of the assembly, which was established by comparing LVDT and strain gage data acquired simultaneously during the elastic deformation of a 416 martensitic steel calibration sample.

For elevated-temperature tests, annealed samples were heated within a forced-convection air furnace at a rate of 5 K·min^{-1} to a temperature 20 K above their zero-stress A_f temperature. The system was equilibrated at A_f + 20 K for 10 minutes, cooled to test temperature, and held for 15 minutes before testing. Temperature was monitored by three K-type thermocouples glued on the specimen and the two carbide disks: within the thermocouple accuracy of 1.5 K, no thermal gradients were detected during testing.

III. RESULTS

A. *Materials*

As expected from their titanium-rich composition, measured as 51.39 ± 0.34 at. pct Ti in Reference 19, the materials are martensitic at room temperature.[5,6] Transformation temperatures of annealed specimens from batch 1 (Table I) are similar to those measured in a previous investigation.[19] The density of the annealed NiTi specimens (Table I) is close to the theoretical value of 6.45 g·cm^{-3}.[27] Figure 1 confirms that the material is pore-free and shows prior powder surfaces (which were invisible in the unetched condition), indicating some surface contamination of the sprayed powders. The very fine structure observed within the bulk probably represents martensitic variants. As shown in Figure 2, the particle-matrix interface in NiTi-10TiC composites is unreacted and pore-free. While slight porosity is visible within the TiC particles, the matrix is fully densified, as confirmed by the close agreement between the measured density and the theoretical value (Table I), calculated from the rule of mixture with a density of 4.93 g·cm^{-3} for TiC.[28] However, density of the NiTi-20TiC composites is significantly less than predicted by the rule of mixture due to porosity in the vicinity of the NiTi-TiC interface. A uniform distribution of the TiC particles was observed in both composite materials.

B. *Mechanical Properties*

A typical stress-strain curve for NiTi is shown in Figure 3 with compressive engineering stress and strain plotted as positive values, a convention followed throughout this article. Because porosity reduces the effective load-bearing area of the specimens, the stress is corrected by dividing the nominal stress by the dimensionless density given in Table I. Although several deformation mechanisms contribute simultaneously to strain, dominant mechanisms can be separated into the five regions shown in Figure 3. On loading in region A, elastic deformation of the initial structure takes place, which, at high temperature, consists of austenite β and at low temperature of martensite M, formed of

Table I. Transformation Temperatures of Annealed Samples from Batch 1 Determined by Calorimetry and Sample Density Determined by Water Displacement

	NiTi	NiTi-10TiC	NiTi-20TiC
A_s (K)	365	362	358
A_f (K)	385	383	384
M_s (K)	347	348	346
M_f (K)	337	334	330
Density (batch 1) (pct)	98.6	97.1	92.6
Density (batch 2) (pct)	99.4	98.8	90.6

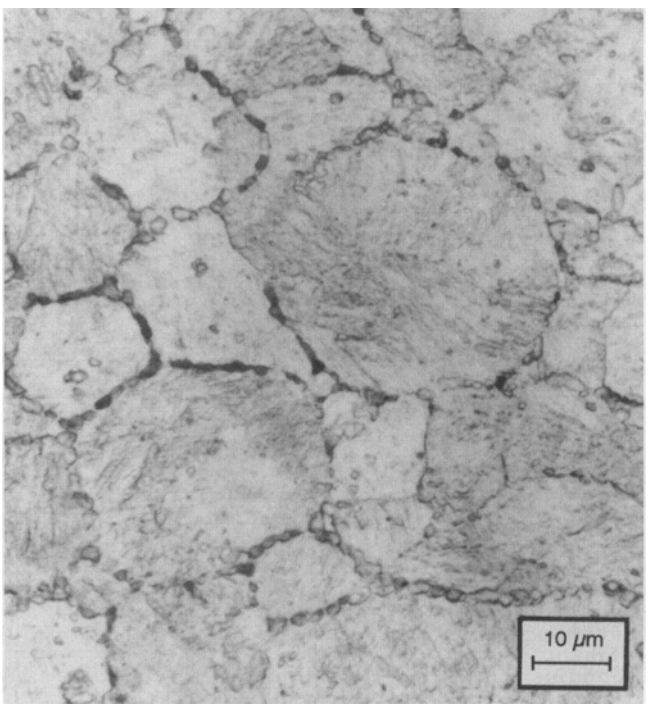

Fig. 1—Micrograph of etched NiTi, showing prior surface of metallic powder and fine martensitic structure.

equal fractions of the 24 possible variants. Region B corresponds to formation of oriented martensite M' containing a majority of variants favorably oriented with respect to the loading axis, which, depending on the initial crystal structure (β or M), are formed either by stress-induced transformation ($\beta \rightarrow M'$) or by stress-induced reorientation, *i.e.*, twinning ($M \rightarrow M'$).[29–33] Deformation in region C includes contributions of both region B and region D (elastic and plastic deformation by slip of oriented martensite M' or retained austenite).[30,34,35] Finally, upon unloading in region E, elastic recovery and some reversion of oriented M' are responsible for strain recovery.[20] The nomenclature used for the slopes and end-points of these regions is given in Figure 3.

The crystal structure (β or M) of NiTi prior to mechanical loading governs the deformation mechanisms and, thus, the overall mechanical behavior during deformation. Three sets of experiments were performed on samples from batch 1, with varying deformation temperatures T_d and thus different zero-stress crystal structures of the NiTi matrix. First, Figure 4 shows the stress-strain behavior of samples tested

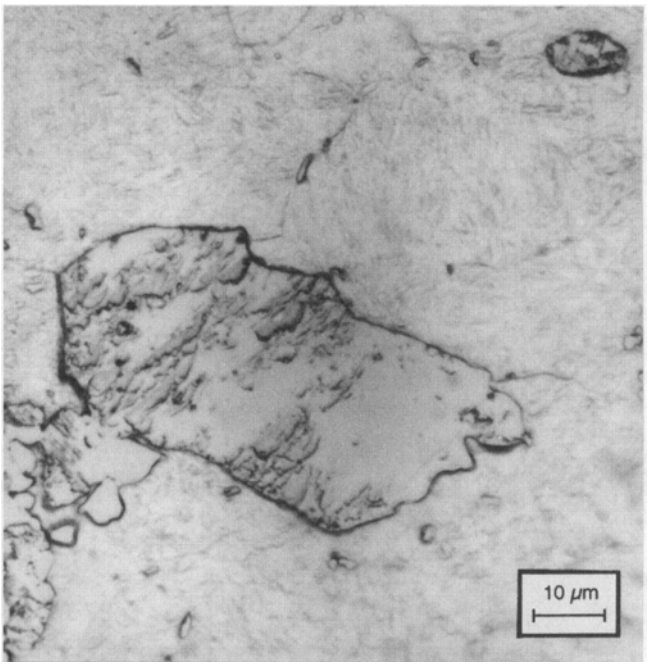

Fig. 2—Micrograph of etched NiTi-10TiC, showing unreacted, well-bonded interface between the NiTi matrix and the TiC particles.

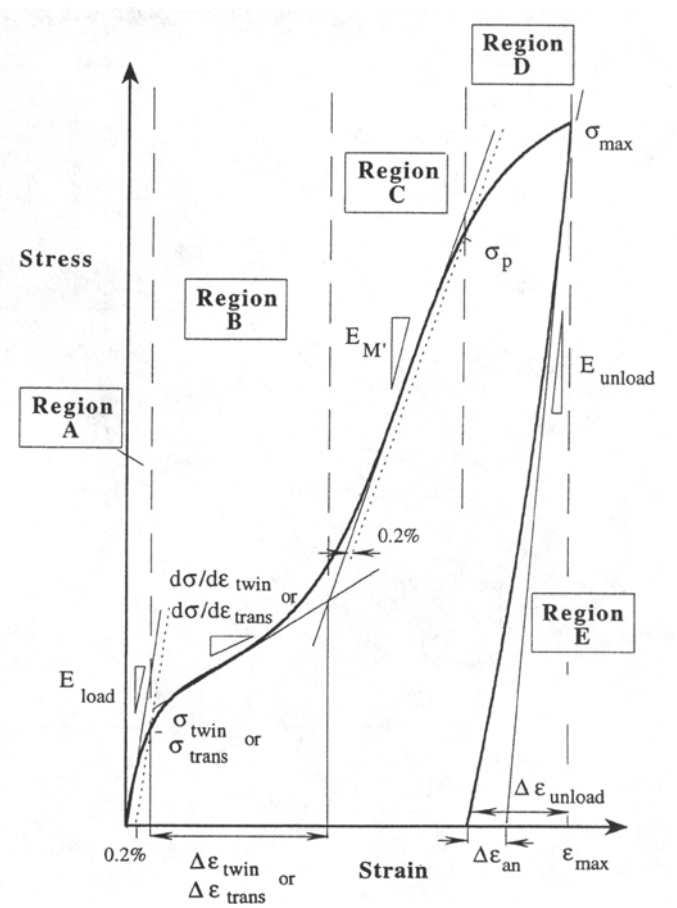

Fig. 3—Schematic compression stress-strain curve for NiTi, with different deformation regions and corresponding nomenclature.

at $T_d = A_f + 5$ K (388 to 390 K, Table I) after cooling from $A_f + 20$ K; at this testing temperature, austenite is chemically stable in the unstressed condition. Second, Fig-

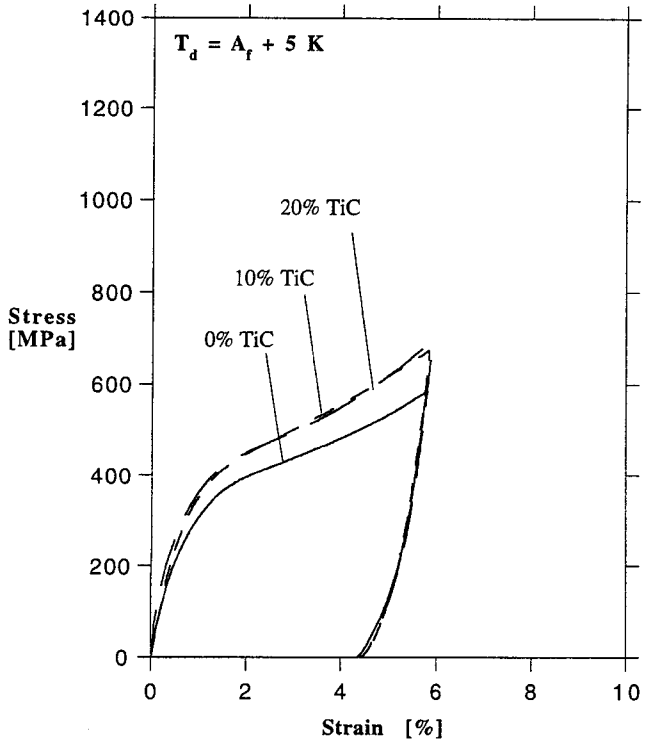

Fig. 4—Stress-strain curve of NiTi and NiTi-TiC composites tested at $T_d = A_f + 5$ K after cooling from $A_f + 20$ K.

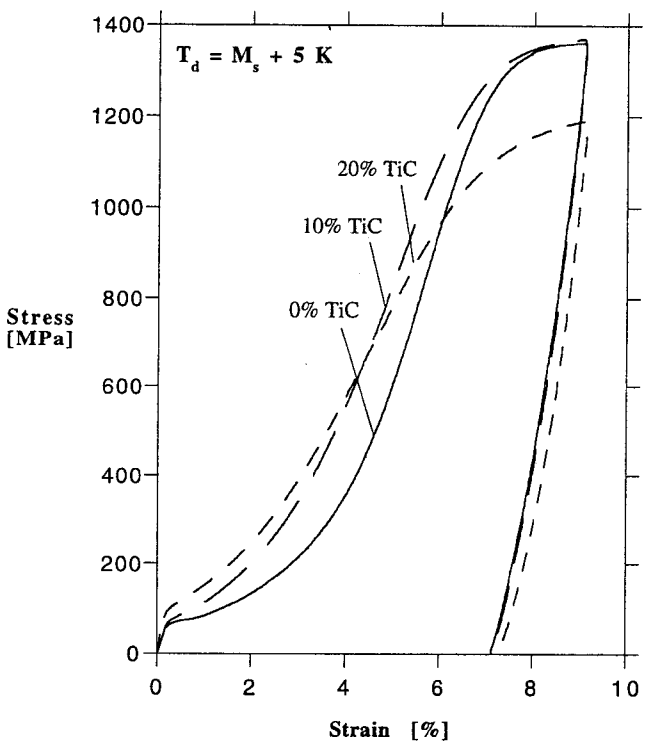

Fig. 5—Stress-strain curve of NiTi and NiTi-TiC composites tested at $T_d = M_s + 5$ K after cooling from $A_f + 20$ K.

ure 5 displays the stress-strain curves of samples first heated to a fully austenitic state at a temperature of $A_f + 20$ K and then cooled to the deformation temperature $T_d = M_s + 5$ K (351 to 353 K). Since this deformation temperature lies below the A_s temperature (A_s = 358 to 365 K), the undeformed structure consists of metastable austenite. Third,

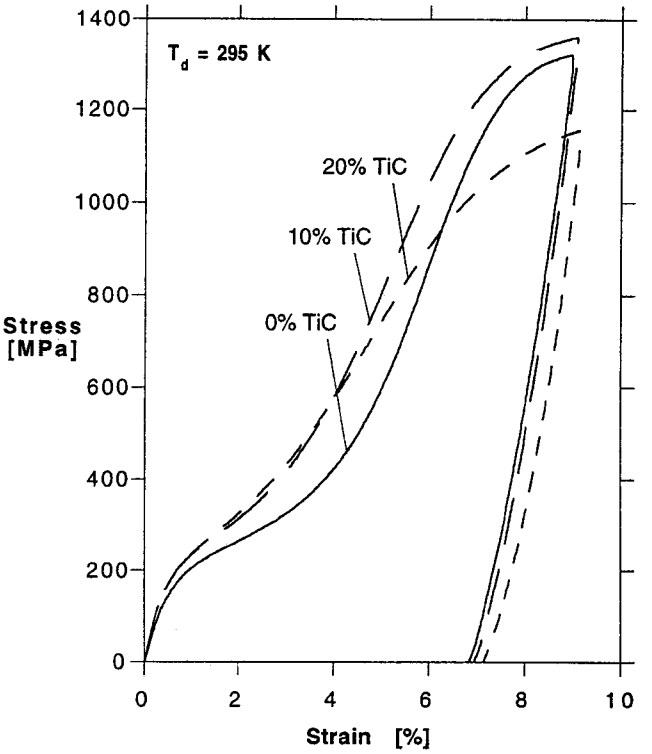

Fig. 6—Stress-strain curve of NiTi and NiTi-TiC composites tested at room temperature.

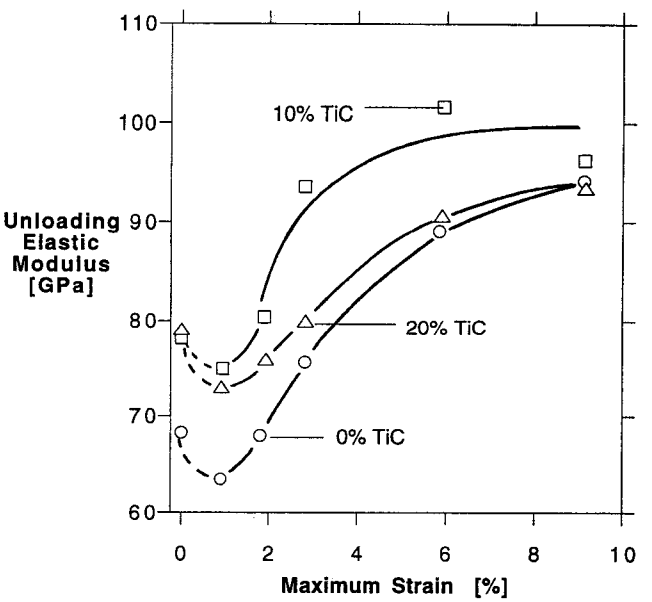

Fig. 7—Initial apparent elastic modulus upon unloading E_{unload} of samples from batch 2 deformed at room temperature up to different maximum strains. The values at 0 pct strains correspond to the loading modulus.

Figure 6 shows the stress-strain curves of martensitic samples deformed at room temperature far below the M_f temperature (M_f = 330 to 337 K), where martensite is stable.

Martensitic samples from batch 2 were deformed at room temperature to a series of strain values between about 1 and 9 pct to investigate the effect of prestrain on both mechanical unloading behavior, as discussed subsequently, and thermal recovery, as reported elsewhere.[21,36] The apparent elastic modulus upon unloading E_{unload}, given in Figure 7, increases with increasing prestrain. The total strain recovery

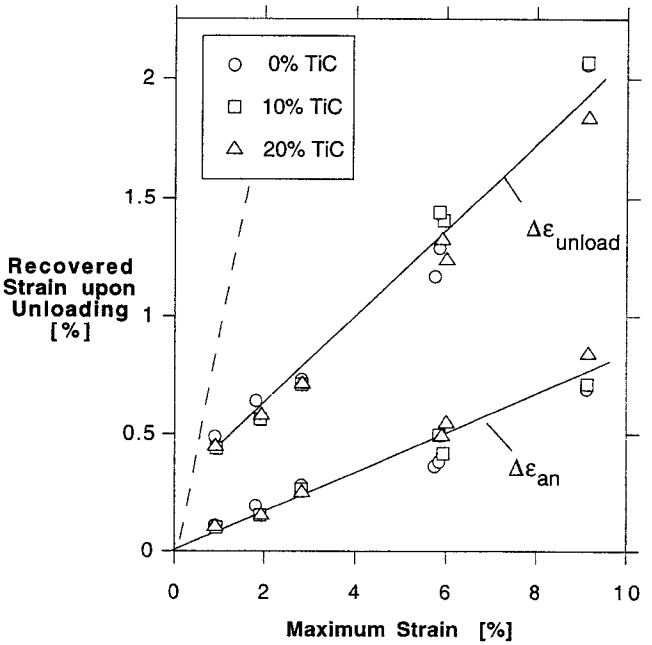

Fig. 8—Total strain recovery $\Delta\varepsilon_{unload}$ and anelastic strain recovery $\Delta\varepsilon_{an}$ (rubberlike recovery) upon unloading at room temperature as a function of the maximum applied strain.

upon unloading $\Delta\varepsilon_{unload}$ is the sum of the elastic strain and an anelastic contribution $\Delta\varepsilon_{an}$. The values of $\Delta\varepsilon_{unload}$ and $\Delta\varepsilon_{an}$, given in Figure 8, increase linearly with an increasing maximum loading strain. While the materials show some rubberlike recovery upon unloading, the anelastic recovery strains represent only about 10 pct of the total recoverable strain, represented by a dotted line in Figure 8.

IV. DISCUSSION

The porosity for NiTi-20TiC is significantly larger than for NiTi-10TiC. The retarding effect of rigid inclusions on the uniaxial densification kinetics of metal powders increases with increasing content of rigid inclusions, as a result of lower initial density and load shielding by the particles.[37,38] The latter effect is expected to increase strongly when the rigid particles form a continuous contacting network, at volume fractions of about 16 pct.[38] We assume in the following that the effect of porosity on the mechanical properties is negligible, except for the reduction of load-bearing area taken into account by correcting the effective cross-sectional area of the samples. However, mismatch stresses and load transfer between particle and matrix may be altered by interfacial porosity. Furthermore, the additional free surface at matrix pores allows unconstrained transformation of the variants in contact with the pores, while stress concentration near pores may induce transformation at reduced external stresses.

Residual internal stresses have been shown to influence the mechanical behavior of metal matrix composites deforming by slip (*e.g.*, References 39 and 40.) As reported in companion articles,[19,20] the calculated residual stresses, resulting from thermal and transformational mismatch between NiTi and TiC after cooling from annealing temperature, are small. Neutron diffraction experiments confirmed that no measurable difference in residual stresses exists between NiTi and NiTi-20TiC at room temperature.[20] We therefore assume in the present study that any difference in the stress-strain curves between unreinforced and reinforced NiTi is due to mismatch stresses and strains between matrix and particles resulting from mechanical deformation, rather than due to thermal or transformational mismatch stresses resulting from processing.

A. *Austenitic Samples Deformed at Elevated Temperature*

1. *NiTi*

At the deformation temperature $T_d = A_f + 5$ K, the unstressed samples consist of the stable, austenitic β phase. The presence of regions B and C in the stress-strain curve (Figure 4) is only possible if the slip yield stress σ_p is higher than the transformation yield stress σ_{trans}. The slip yield stress σ_p is independent of temperature for NiTi below 400 °C,[41,42] while the transformation yield stress σ_{trans} increases rapidly with increasing temperature T, according to the Clausius–Clapeyron relationship (*e.g.*, References 43 and 44):

$$\frac{\Delta\sigma_{trans}}{\Delta T} = \frac{\rho \cdot \Delta H}{\Delta\varepsilon \cdot T_0} \qquad [1]$$

where ρ is the density, ΔH is the transformation enthalpy, T_0 is the chemical equilibrium temperature, and $\Delta\varepsilon$ is the strain resulting from the transformation in the direction of the applied uniaxial stress.

Of the two possible deformation mechanisms in region B of Figure 4, *i.e.*, slip and stress-induced transformation, the latter is the most likely for the following reasons. First, the positive curvature of the stress-strain curves at a strain of about 4 pct indicates the onset of another deformation mechanism (region C) and cannot be explained by slip. Second, positive curvature in the unloading portion of the curve is characteristic of martensite undergoing reverse twinning (rubberlike recovery) or reverse transformation (superelastic recovery). Finally, the 0.2 pct proof stress measured in Figure 4 (σ = 243 MPa) is significantly lower than the tensile slip yield stress in austenitic NiTi with similar A_f temperature, which is on the order of 400 MPa.[42]

After cooling from $A_f + 20$ K to the deformation temperature $T_d = M_s + 5$ K, the undeformed samples are austenitic. Region B of the stress-strain curve of these samples (Figure 5) is expected to correspond to the formation of stress-induced martensite, as for the samples deformed at $T_d = A_f + 5$ K (Figure 4), because the transformation yield stress σ_{trans} decreases with decreasing temperature (Eq. [1]). Using values of $\rho = 6.45$ g·cm^{-3},[27] the approximations $\Delta H = 32.5$ kJ·kg^{-1} and $T_0 = 1/2\ (M_s + A_f) = 366$ K discussed in an earlier article,[19] and $\Delta\varepsilon = 0.052$ as calculated by Saburi and Nenno[3] for the maximum transformation strain in compression, Eq. [1] predicts a value $\Delta\sigma_{trans}/\Delta T = 11$ MPa·K^{-1}. With the parameter $\Delta\varepsilon = 0.106$ calculated for tensile deformation,[3] Eq. [1] yields $\Delta\sigma_{trans}/\Delta T = 5.4$ MPa·K^{-1}. Because, due to strain compatibility, the most favorable stress-induced variants cannot be the same in polycrystalline samples as in single crystals, the expected values for $\Delta\sigma_{trans}/\Delta T$ are expected to be situated between those calculated in compression and in tension. The value derived for NiTi from Figures 4 and 5, $\Delta\sigma_{trans}/\Delta T = 4.7$ MPa·K^{-1} (Table II), is at the lower range of the values calculated previously but falls within the large span of experimental

Table II. Transformation Yield Stress σ_{trans} and Clausius–Clapeyron Slope $\Delta\sigma_{trans}/\Delta T$ for all Samples from Batch 1 Tested above Room Temperature

	σ_{trans} (MPa) at A_f + 5K		σ_{trans} (MPa) at M_s + 5K		$\Delta\sigma_{trans}/\Delta T$ (MPa · K^{-1})	
	Measured	Eq. [2]	Measured	Eq. [2]	Measured	Eq. [5]
NiTi	243	243*	66	66*	4.7	4.7*
NiTi-10TiC	285	266	76	72	6.0	5.2
NiTi-20TiC	320	290	109	79	5.6	5.6

*Assumed equal to the measured value.

Table III. Elastic Modulus upon Loading E_{load} and Twinning Yield Stress σ_{twin}, Averaged for All Samples from Batch 2 Tested at Room Temperature with Strain Gages

	E_{load} (GPa)		σ_{twin} (MPa)	
	Measured	Predicted (Eq. [6])	Measured	Predicted (Eq. [2])
NiTi	68	68*	180	180*
NiTi-10TiC	78	80	180	197
NiTi-20TiC	79	94	186	215

*Assumed equal to the measured value.

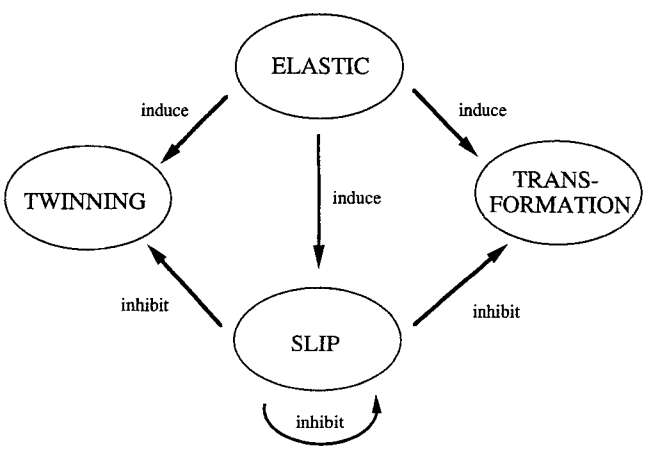

Fig. 9—Schematic relationships between the deformation mechanisms operative in NiTi.

values for polycrystalline NiTi tested in tension, ranging from 3.3 to 13 MPa·K^{-1}.[27,30,42,45–50]

2. *NiTi-TiC Composites*

As shown in Table II and Figures 4 and 5, the transformation yield stress σ_{trans}, corresponding to the onset of generalized formation of stress-induced martensite M', increases with increasing TiC content. We first determine if this effect can be explained by load transfer between the compliant matrix and the stiff particles by using the Eshelby theory. As described in Reference 39 for the case of a matrix deforming by slip, generalized yielding in the composite occurs at an applied stress σ_{yc} for which the matrix average stress in the composite is equal to the slip yield stress of the unreinforced matrix, σ_y. Strengthening is described by a parameter P,

$$\sigma_{yc} = \frac{\sigma_y}{P} \quad [2]$$

determined from the Tresca yield criterion as

$$P = 1 + \frac{\langle\sigma_3\rangle_m - \langle\sigma_1\rangle_m}{\sigma_A} \quad [3]$$

where σ_A is the applied stress and the mean matrix stress tensor $\langle\sigma\rangle_m$ is given by Eshelby's theory as

$$\langle\sigma\rangle_m = -fC_m(S-I)\{(C_m - C_i)[S - f(S-I)] - C_m\}^{-1}(C_i - C_m)C_m^{-1}\sigma_A \quad [4]$$

where C is the stiffness tensor, S the Eshelby tensor, I the identity tensor, f the volume fraction, and the subscripts m and i correspond to the matrix and inclusion, respectively.

Assimilating σ_y to σ_{trans} and introducing Eq. [2] into the Clausius–Clapeyron relationship (Eq. [1]) gives, for the composite transformation yield stress $\sigma_{trans,c}$,

$$\frac{\Delta\sigma_{trans,c}}{\Delta T} = \frac{1}{P}\cdot\frac{\rho\cdot\Delta H}{\Delta\varepsilon\cdot T_0} \quad [5]$$

Equations [3] and [4] give values of $P = 0.912$ for NiTi-10TiC and $P = 0.838$ for NiTi-20TiC, assuming spherical TiC particles with elastic constants given in Reference 51 and using for NiTi the measured Young's modulus (Table III) and a Poisson's ratio $\nu = 0.35$[52] under a cubic assumption. As shown in Table II, while the experimental temperature dependence of the transformation yield stress $\Delta\sigma_{trans,c}/\Delta T$ is in reasonable agreement with Eq. [5] for both composites, the observed yield values $\sigma_{trans,c}$ are significantly higher than predicted by Eq. [2].

This discrepancy indicates that the assumption made previously (*i.e.*, the intrinsic twinning yield stress of the matrix σ_{trans} is unaffected by the particles) may not hold. Indeed, for composites deforming by slip, the 0.2 pct proof stress of the composite matrix is often higher than that of the unreinforced matrix, as a result of forest hardening by dislocations punched to relax the elastic and plastic mismatches between the two phases.[53,54,55] We propose that a similar effect is occurring in austenitic NiTi composites, increasing the matrix intrinsic twinning stress σ_{trans} (also determined at a plastic strain of 0.2 pct, Figure 3). While most of the particle-matrix mismatch can be accommodated in the early stage of deformation by stress-induced transformation, it is likely that the slip yield stress is exceeded at stress concentration points at the NiTi-TiC interface, so that dislocations are punched into the matrix. As shown by References 46, 56, and 57 for NiTi deformed by slip, dislocations stabilize the austenite by preventing the motion of interfaces. Therefore, the austenitic matrix of the NiTi-TiC composites with high density of punched dislocations is expected to exhibit a transformation yield stress $\sigma_{trans,c}$ higher than predicted by Eq. [2]. The effect of elastic stresses on the two competing plastic mechanisms (slip and stress-induced transformation) and the interaction between these mechanisms are schematically shown in Figure 9.

The hypothesis that mismatch dislocations stabilize the austenitic matrix is corroborated by the mechanical behavior of the composites at $T_d = M_s + 5$ K (Figure 5), for which the following trends are found as the fraction of TiC particles increases. First, the strain resulting from transformation $\Delta\varepsilon_{trans}$ decreases, indicating that a smaller fraction

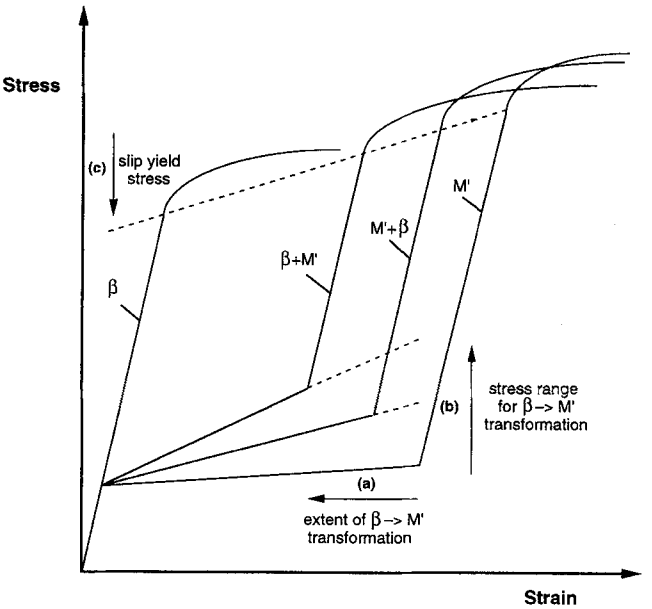

Fig. 10—Schematic effect on the stress-strain curve of NiTi of austenite stabilization by TiC for an initially austenitic sample β deforming by formation of stress-induced martensite M' ($\beta \rightarrow M'$): (a) decrease of total transformation strain, (b) increase of transformation stress range, and (c) decrease of slip yield stress. The curve M' corresponds to a sample undergoing complete formation of martensite and the curve β to a fully stabilized austenitic sample. If β is replaced by M, the same figure applies for a martensitic sample M deforming by twinning ($M \rightarrow M'$), where M is stabilized by TiC particles.

of stress-induced martensite M' is formed in region B. Second, the slope $d\sigma/d\varepsilon_{trans}$ increases in region B (an effect also observed at A_f + 5 K) and the slope $E_{M'}$ decreases in region C, indicating a larger range of stresses over which M' is forming, as expected if austenite is stabilized; this is similar to the enhanced strain hardening observed in many metal matrix composites deforming by slip, whereby secondary dislocations punched by particles interfere with the glide of primary dislocations and strengthen the matrix by forest hardening.[53,54,55] Third, the slip yield stress σ_p in region D decreases markedly for NiTi-20TiC. Since σ_p is lower in the austenite than in the martensite,[42] the preceding observation confirms that a larger fraction of retained austenite exists in NiTi-20TiC. The three effects described previously are illustrated in Figure 10, in which each region is assumed to exhibit a single deformation mechanism, as reflected by the sharp transitions in the stress-strain curves. In actuality, the deformation mechanisms overlap from one region to the other, resulting in the smooth transitions between regions found in Figures 4 and 5.

Superelastic recovery ($M' \rightarrow \beta$) is not expected upon unloading, because stress-induced martensitic phase M' is stable (either intrinsically at $T_d = M_s + 5$ K or because it is strain stabilized at $T_d = A_f + 5$ K[21,36]). The small anelastic strain measured upon unloading (Figures 4 and 5) can thus be assigned to rubberlike recovery ($M' \rightarrow M$), driven during unloading by the internal stresses resulting from the mismatch of elastic constants between anisotropic variants within the matrix or between matrix and reinforcement. No significant difference in the extent of anelastic recovery is observed in Figures 4 and 5 as the TiC content is varied. This indicates that the internal stresses upon unloading are not significantly affected by the particles, either because the TiC particles do not alter the state of stress or because the mismatch stresses are relaxed by localized twinning or slip, not affecting the overall macroscopic behavior. As shown later, the second hypothesis is retained to explain the behavior of the martensitic-reinforced NiTi samples deformed at room temperature.

B. *Martensitic Samples Deformed at Room Temperature*

1. *NiTi*

The compression curve of NiTi at room temperature (Figure 6) exhibits a shape similar to that published by Wasilewski,[58] who reported that region B in NiTi is much shorter in compression than in tension. Except for the value of the stress at the onset of region B, the stress-strain characteristics of the martensitic sample at room temperature (Figure 6) are very similar to those of the austenitic sample at M_s + 5 K (Figure 5). However, the dominant deformation mechanisms in region B are different: in contrast to stress-induced formation of martensite ($\beta \rightarrow M'$) taking place at elevated temperature, as discussed previously (Figure 5), twinning ($M \rightarrow M'$) occurs at room temperature (Figure 6). The 24 randomly oriented martensitic variants M coalesce into one or more optimally oriented variants M', as observed by neutron diffraction in a companion article.[20] The similarity of the stress-strain curves in regions C through E between the samples deformed at elevated temperature (Figure 5) and at room temperature (Figure 6) is expected, since in both cases, the same majority phase M' is deforming, independently of its parent phase.

The unloading behavior (region E) was examined for samples in batch 2 deformed to varying strains: 1, 2, and 3 pct within region B (twining deformation regime), 6 pct within region C (transition regime), and 9 pct within region D (slip deformation regime). Figure 7 shows a systematic increase in unloading modulus E_{unload} with increasing strain, leveling out in region C to a value of about E_{unload} = 95 GPa, as also observed in unreinforced NiTi by Wasilewski.[58] Since twinning during compressive deformation leads to preferential orientation of (100) planes perpendicular to the loading axis,[20] and since the constrained Young's modulus in the direction perpendicular to the (100) planes is about 120 GPa,[20] an increase of elastic modulus is indeed expected with increasing twinning strain.

Finally, the anelastic recovery $\Delta\varepsilon_{an}$ upon unloading increases linearly with the maximum strain ε_{max} (Figure 8). Because reverse twinning is expected to increase with mismatch, the increase of $\Delta\varepsilon_{an}$ in Figure 8 indicates that the internal mismatch stresses upon unloading increase with deformation.

2. *NiTi-TiC Composites*

Assuming that elastic load transfer from the matrix to spherical particles is operative, the composite stiffness tensor C_c can be predicted by Eshelby's theory:[39]

$$C_c = \left[C_m^{-1} - f\{(C_i - C_m)[S - f(S - I)] + C_m\}^{-1}(C_i - C_m)C_m^{-1}\right]^{-1} \quad [6]$$

As discussed in more detail in a companion publication,[20] the macroscopic loading elastic modulus of unreinforced NiTi E_M measured by strain gage is somewhat smaller than that measured by neutron diffraction due to small amounts of twinning initiated in the apparent elastic region. With an

apparent elastic modulus E_M = 68 GPa and other material constants given in Reference 20, Eq. [6] predicts composite elastic moduli values given in Table III, which also lists the experimental values measured by strain gage. For an experimental error estimated at about ±3 GPa (a relatively high value due to the narrow range of the linear region), the measured elastic modulus for NiTi-10TiC is in agreement with that calculated by Eq. [6]. However, as also observed in another investigation,[20] the elastic modulus of NiTi-20TiC is significantly smaller than predicted by Eq. [6]. It is concluded that in NiTi-10TiC, stiffening results from load transfer from the matrix to the TiC particles without creation of mismatch stresses exceeding the twinning yield stress σ_{twin}, which would induce significant additional matrix twinning and a lower apparent elastic modulus. On the other hand, in NiTi-20TiC, stiffening by load transfer to the TiC particles is partially canceled by the additional twinning resulting from relaxation of elastic incompatibility between matrix and reinforcement (Figure 9).

The twinning yield stress values in Table III confirm that additional twinning is taking place in the composites. The measured value σ_{twin} is independent of the volume fraction TiC, in disagreement with the prediction of Eq. [2] based on load transfer without relaxation. As proposed in a companion article,[20] relaxation by twinning of the mismatch stresses between matrix and particles explains that observation. This behavior is different from that of the austenitic samples described previously, whereby mismatch relaxation by slip strengthens the matrix and results in transformation yield stress values σ_{trans} higher than predicted by Eq. [2] (Section A–2).

We now discuss the room-temperature stress-strain curves (Figure 6) at higher strains. With increasing fractions of TiC particles, the curves exhibit the same trends as observed at the deformation temperature of M_S + 5 K (Figure 5): increases of σ_{twin} and $d\sigma/d\varepsilon_{twin}$ as well as decreases of Δe_{twin}, $E_{M'}$, and σ_p. Similar to the stabilization of austenite β discussed earlier for the curves at M_s + 5 K, these observations can be explained by the stabilization of martensite M, as TiC particles prevent twinning ($M \rightarrow M'$) at strains above about 2 pct (Figure 10). Dislocations created to accommodate the *plastic* mismatch between the matrix and reinforcement are expected to stabilize the martensitic matrix, similar to the inhibition of twinning by dislocations exerting a friction stress on the moving twin boundaries reported by References 46, 56, 59, and 60. The significant decrease of σ_P observed in NiTi-20TiC can further be understood if NiTi-20TiC contains significant amounts of M. The slip yield stress is expected to be lower for M than for M', because dislocations created by twinning will induce hardening of M'.

In summary, we propose that two mechanisms are operative to relax elastic mismatch stresses in the composites upon loading at room temperature (Figure 9), each with opposite effects on the twinning behavior of the matrix. At low strains, mismatch between NiTi and TiC is relaxed by twinning, leading to an apparent elastic modulus and a yield stress lower than expected. At higher strains, some of the mismatch is also relaxed by slip and the resulting dislocations inhibit further large-scale twinning of the matrix.

As for unreinforced NiTi, the unloading elastic modulus of the composites increases with increasing prestrains (Figure 7). Furthermore, with increasing TiC volume fraction, the same trends are found for the unloading modulus as for the loading modulus. First, for NiTi-10TiC, the unloading modulus increases in good quantitative agreement with load transfer theory (Eq. [6]), except for the highest prestrain. Second, NiTi-20TiC exhibits very little stiffening as compared to unreinforced NiTi for all prestrains, probably because mismatch stresses between particle and matrix are high enough to significantly assist early reverse twinning.

As shown in Figure 8 (and as also reported in a companion article) for a single strain value[20], the total anelastic strain recovery $\Delta\varepsilon_{an}$ is independent of TiC content. This indicates that while the mismatch stresses from TiC particulates are sufficient to alter the apparent elastic unloading slope, these stresses do not influence significantly the magnitude of the strain of the rubberlike recovery of the material, a result also observed in unloading of austenitic samples and discussed earlier. As reported in a companion article,[20] the extent of reverse twinning for specific crystallographic planes is different between the unreinforced and composite NiTi, but the internal stresses are near zero in the unloaded condition for both materials. We thus conclude that the high degree of liberty offered by twinning allows the complete relaxation of unloading mismatch stresses without a measurable difference in the total macroscopic reverse twinning strain.

V. CONCLUSIONS

The compressive stress-strain behavior of NiTi with 0, 10, and 20 vol pct TiC particulates was investigated up to high strains at different temperatures. The goal was to examine the mechanical behavior of metal matrix composites deforming by mechanisms other than slip, *i.e.*, matrix twinning ($M \rightarrow M'$) for martensitic composites at low temperature and matrix stress-induced transformation ($\beta \rightarrow M'$) for austenitic composites at elevated temperature. The effect of particles can be summarized as follows.

1. For an austenitic matrix, the transformation yield stress σ_{trans} is higher than predicted by Eshelby's load transfer theory. Furthermore, compared to unreinforced NiTi, the range of stress for formation of martensite M' in the composites is increased and the maximum fraction of M' is lowered. These effects can be rationalized if dislocations, created by the plastic relaxation of mismatch between matrix and particles, stabilize the austenitic matrix β and prevent the formation of M'. However, the yield stress for slip σ_p is lower for the composites, because they contain more austenite β which is weaker than martensite M'.
2. For a martensitic matrix, the twinning yield stress σ_{twin} and the apparent elastic modulus are less than predicted by Eshelby's load transfer theory. This can be explained by twinning relaxation of the elastic mismatch between matrix and reinforcement. At higher strains, however, the total volume of twinned martensite M' is lower and the stress range for M' formation is higher for the composites than for unreinforced NiTi. Similar to the austenitic composites, dislocations created by the relaxation of the mismatch between matrix and particles can prevent twinning and thus strengthen the martensitic matrix in the region where twinning is the main deformation

mechanism. Finally, the slip yield stress σ_p is lower for the composite, because the weaker M is stabilized.

3. The extent of strain recovery upon unloading by rubberlike recovery (reverse twinning $M' \rightarrow M$) is unaffected by the particles, indicating that the mismatch created upon unloading is fully accommodated by the matrix.

ACKNOWLEDGMENTS

This research was supported, in part, by the National Science Foundation Materials Research Laboratory (Grant No. DMR90-22933), administrated through the Center for Materials Science and Engineering, MIT. DM and DCD acknowledge the support of the Swiss National Foundation, in the form of a postdoctoral grant, and of AMAX, in the form of an endowed chair at MIT, respectively.

REFERENCES

1. C.M. Wayman: *Met. Forum*, 1981, vol. 4, pp. 135-41.
2. J. Perkins: *Met. Forum*, 1981, vol. 4, pp. 153-63.
3. T. Saburi and S. Nenno: in *Solid-Solid Phase Transformations*, H.I. Aaronson, D.E. Laughlin, R.F. Sekerka, and C.M. Wayman, eds., TMS-AIME, Warrendale, PA, 1982, pp. 1455-79.
4. K. Otsuka and K. Shimizu: *Int. Met. Rev.*, 1986, vol. 31, pp. 93-114.
5. K. Shimizu and T. Tadaki: in *Shape Memory Alloys*, H. Funakubo, ed., Gordon and Breach, New York, NY, 1987, pp. 1-60.
6. T. Honma: in *Shape Memory Alloys*, H. Funakubo, ed., Gordon and Breach, New York, NY, 1987, pp. 61-115.
7. C.M. Wayman and J.D. Harrison: *J. Met.*, 1989, vol. 41, pp. 26-28.
8. E. Hornbogen: in *Progress in Shape Memory Alloys*, S. Euken, ed., DGM, Oberursel, Germany, 1992, pp. 3-19.
9. D. Goldstein and S.M. Hoover: U.S. Patent No. 5,145,506, 1992.
10. S.N. Kul'kov, T.M. Poletika, A.Y. Chukhlomin, and V.E. Panin: *Poroshkovaya Metall.*, 1985, vol. 8 (260), pp. 652-55.
11. T.M. Poletika, S.N. Kul'kov, and V.E. Panin: *Poroshkovaya Metall.*, 1983, vol. 7 (247), pp. 560-64.
12. Y. Yamada: *Phys. Rev.*, 1992, vol. 46, pp. 5906-11.
13. Y. Furuya, A. Sasaki, and M. Taya: *Mater. Trans. JIM*, 1993, vol. 34, pp. 224-27.
14. J.E. Bidaux, J.A.E. Manson, and R. Gotthardt: in *First International Conference on Shape Memory and Superelastic Technologies*, A.R. Pelton, D. Hodgson, and T. Duerig eds., MIAS, Monterey CA, 1995, pp. 37-42.
15. K. Escher and E. Hornbogen: *J. Phys. IV*, 1991, vol. 1, pp. C4-427-C4-432.
16. E. Hornbogen, M. Thumann, and B. Velten: in *Progress in Shape Memory Alloys*, S. Eucken ed., DGM, Oberursel, Germany, 1992, pp. 225-36.
17. T.W. Duerig and K.N. Melton: in *The Martensitic Transformation in Science and Technology*, E. Hornbogen and N. Jost, eds., DGM, Oberursel, Germany, 1989, pp. 191-98.
18. L.C. Zhao, T.W. Duerig, S. Justi, K.N. Melton, J.L. Proft, W. Yu, and C.M. Wayman: *Scripta Metall. Mater.*, 1990, vol. 24, pp. 221-26.
19. D. Mari and D.C. Dunand: *Metall. Mater. Trans. A*, 1996, vol. 27A, pp. 0000-00.
20. D.C. Dunand, D. Mari, M.A.M. Bourke, and J.A. Roberts: *Metall. Mater. Trans. A*, in press.
21. K.L. Fukami-Ushiro and D.C. Dunand: *Metall. Mater. Trans. A*, 1996, vol. 27A, pp. 193-203.
22. R.W.K. Honeycombe: *The Plastic Deformation of Metals*, Edward Arnold Publishers Ltd., London, 1984, pp. 204-20.
23. M.A. Meyers and K.K. Chawla: *Mechanical Metallurgy Principles and Applications*, Prentice-Hall, Englewood Cliffs, NJ, 1984, pp. 467-90.
24. C.H. Vasel, A.D. Krawitz, E.F. Drake, and E.A. Kenik: *Metall. Trans. A*, 1985, vol. 16A, pp. 2309-17.
25. R. Schaller, D. Mari, M. Maamouri, and J.J. Ammann: *J. Hard Mater.*, 1992, vol. 3, pp. 351-62.
26. D. Mari and D.R. Gonseth: *Wear*, 1993, vol. 165, pp. 9-17.
27. C.M. Jackson, H.J. Wagner, and R.J. Wasilewski: NASA-SP 5110, 1972, pp. 23-74.
28. *The CRC Materials Science and Engineering Handbook*, J. Shackelford and W. Alexander, eds., CRC Press, Boca Raton, FL, 1992, p. 436.
29. F. Takei, T. Miura, S. Miyazaki, S. Kimura, K. Otsuka, and Y. Suzuki: *Scripta Metall.*, 1983, vol. 17, pp. 987-92.
30. S. Miyazaki, K. Otsuka, and Y. Suzuki: *Scripta Metall.*, 1981, vol. 15, pp. 287-92.
31. S. Miyazaki, S. Kimura, K. Otsuka, and Y. Suzuki: *Scripta Metall.*, 1984, vol. 18, pp. 883-88.
32. T. Saburi, M. Yoshida, and S. Nenno: *Scripta Metall.*, 1984, vol. 18, pp. 363-66.
33. S. Miyazaki, S. Kimura, F. Takei, T. Miura, K. Otsuka, and Y. Suzuki: *Scripta Metall.*, 1983, vol. 17, pp. 1057-62.
34. J. Perkins: *Scripta Metall.*, 1974, vol. 8, p. 1469.
35. K.N. Melton and O. Mercier: *Metall. Trans. A*, 1978, vol. 9A, pp. 1487-88.
36. K.L. Fukami: Master's Thesis, Massachusetts Institute of Technology, Cambridge, MA, 1994.
37. N. Taylor, D.C. Dunand, and A. Mortensen: *Acta Metall. Mater.*, 1993, vol. 41, pp. 955-65.
38. F.F. Lange, L. Atteraas, F. Zok, and J.R. Porter: *Acta Metall. Mater.*, 1991, vol. 39, pp. 209-19.
39. T.W. Clyne and P.J. Withers: *An Introduction to Metal Matrix Composites*, Cambridge University Press, Cambridge, United Kingdom, 1993, pp. 44-165.
40. J.W. Hutchinson and R.M. McMeeking: in *Fundamentals of Metal Matrix Composites*, S. Suresh, A. Mortensen, and A. Needleman, eds., Butterworth-Heinemann, Boston, 1993, pp. 158-73.
41. A.G. Rozner and R.J. Wasilewski: *J. Inst. Met.*, 1966, vol. 94, pp. 169-75.
42. K.N. Melton and O. Mercier: *Acta Metall.*, 1981, vol. 29, pp. 393-98.
43. M. Kato and H.-R. Pak: *Phys. Status Solidi B*, 1984, vol. 123, pp. 415-24.
44. M. Kato and H.-R. Pak: *Phys. Status Solidi B*, 1985, vol. 130, pp. 421-30.
45. S. Miyazaki, Y. Ohmi, K. Otsuka, and Y. Suzuki: *J. Phys.*, 1982, vol. 43, pp. C4-255-C4-260.
46. S. Miyazaki and K. Otsuka: *Metall. Trans. A*, 1986, vol. 17A, pp. 53-63.
47. H. Kato, T. Koyari, M. Tokizane, and S. Miura: *Acta Metall. Mater.*, 1994, vol. 42, pp. 1351-58.
48. H. Tobushi, K. Tanaka, K. Kimura, T. Hori, and T. Sawada: *JSME Int. J.*, 1992, vol. 35, pp. 278-83.
49. P.H. Leo, T.W. Shield, and O.P. Bruno: *Acta Metall. Mater.*, 1993, vol. 41, pp. 2477-85.
50. T. Saburi, T. Tatsumi, and S. Nenno: *J. Phys.*, 1982, vol. 43, pp. C4-261-C4-266.
51. R. Chang and L.J. Graham: *J. Appl. Phys.*, 1966, vol. 37, pp. 3778-83.
52. T.M. Brill, S. Mittelbach, W. Assmus, M. Müllner, and B. Lüthi: *J. Phys. Condensed Matter*, 1991, vol. 3, pp. 9621-27.
53. M.F. Ashby: *Phil. Mag.*, 1970, vol. 21, pp. 399-424.
54. P.B. Prangnell, T. Downes, W.M. Stobbs, and P.J. Withers: *Acta Metall. Mater.*, 1994, vol. 42, pp. 3425-36.
55. A.M. Redsten, E.M. Klier, A.M. Brown, and D.C. Dunand: *Mater. Sci. Eng.*, 1996, vol. A201, pp. 88-102.
56. P. Filip, J. Rusek, and K. Mazanec: *Z. Metallkd.*, 1991, vol. 82, pp. 488-91.
57. P. Filip, J. Rusek, and K. Mazanec: *Mater. Sci. Eng.*, 1991, vol. A141, pp. L5-L8.
58. R.J. Wasilewski: *Metall. Trans.*, 1971, vol. 2, pp. 2973-81.
59. O. Mercier and E. Török: *J. Phys.*, 1982, vol. 43, pp. C4-267-C4-272.
60. H.C. Lin, S.K. Wu, T.S. Chou, and H.P. Kao: *Acta Metall. Mater.*, 1991, vol. 39, pp. 2069-80.